Riemannian Drums, Anisotropic Curve Evolution and Segmentation

Jayant Shah*

Mathematics Department, Northeastern University, Boston, MA 02115.

*This work was partially supported by PHS Grant 2-R01–NS34189–04 from NINDS, NCI and NIMH, and NSF Grant DMS-9531293.

Riemannian Drums

Jayant Shah

Mathematics Department, Northeastern University, Boston, MA 02115.

Tel: 617–373–5660 FAX: 617–373–5658 email: shah@neu.edu

Abstract. The method of curve evolution is a popular method for recovering shape boundaries. However isotropic metrics have always been used to induce the flow of the curve and potential steady states tend to be difficult to determine numerically, especially in noisy or low-contrast situations. Initial curves shrink past the steady state and soon vanish. In this paper, anisotropic metrics are considered to remedy the situation by taking the orientation of the feature gradient into account. The problem of shape recovery or segmentation is formulated as the problem of finding minimum cuts of a Riemannian manifold. Approximate methods, namely anisotropic geodesic flows and solution of an eigenvalue problem are discussed.

.

All symbols should be printed as they appear in the manuscript.

1 Introduction

In recent years, there has been extensive development of methods for shape recovery by curve evolution. These methods are gaining in popularity due to their potential for very fast implementation. A parametric form of it was developed by Katz, Witkin and Terzoupolous [1]. A geometrically intrinsic formulation of active contours was introduced by Caselles, Catte, Coll and Dibos in [2] and developed over the years by several authors [3,4,5,6]. A formulation based on curve evolution introduced by Sethian [7] is also in use where the flow velocity consists of a constant component and a component proportional to the curvature (see for example, [8]). The evolving curve in this case is stopped near the shape boundary or at least slowed by means of a stopping term. From a geometric perspective, the image domain may be viewed as a Riemannian manifold endowed with a metric defined by the image features. An initial curve flows towards a geodesic with normal velocity proportional to its geodesic curvature. Several techniques for fast implemetation of geodesic flows have been developed. The speed of the method is due to two essential factors. First, noise suppression and edge detection are done in a hierarchical fashion: the image is smoothed first and then the geodesic flow is calculated. This is in contrast to the flows defined by segmentation functionals in which noise suppression and edge detection are done simultaneously. The second reason for the speed-up is that the object boundaries are found by tracking one closed curve at a time and thus the computational effort can be focused on a small neighborhood of the evolving curve.

Throughout the development of this approach, the metric used has always been

.

an isotropic metric. In this paper, fully general anisotropic metrics are considered. One reason for developing such a generalization is that in noisy or low contrast situations, the steady states for the isotropic flows are not robust and one has to resort to devices such as a stopping term. For instance, when the image gradient is large everywhere due to noise, curves with the same Euclidean length will have their Riemannian length approximately equal if the metric is isotropic, indicating reduced sensitivity of the method. In practice, the curves tend to continuously shrink and vanish. A way to improve this situation is to take into account the orientation of the gradient by considering anisotropic metrics. Another reason to consider anisotropic metrics comes from the impressive results obtained by Shi and Malik [9] who formulate the problem of shape recovery in natural scenes as a problem of finding the minimum cut in a weighted graph. An ingredient essential for their method to work is the implied anisotropic metric. Finally, use of anisotropic metrics is implied in boundary detection by means of segmentation functionals. This connection is briefly reviewed in Section 2. However its implementation is computationally expensive and it is worthwhile to formulate anisotropic curve evolution directly.

2 Segmentation Functionals and Curve Evolution

Consider the segmentation functional [10]

$$E(u, C) = \int\int_{D\setminus C} \|\nabla u\|^2 dx_1 dx_2 + \mu^2 \int\int_{D} |u - I|^2 dx_1 dx_2 + \nu |C| \qquad (1)$$

where D is the image domain, I is the image intensity, C is the segmenting curve, $|C|$ its length and u is a piecewise smooth approximation of I. Let

$e = \mu^2(u - I)^2 + ||\nabla u||^2$ denote the energy density. Then with u fixed, the gradient flow for C is given by the equation

$$\frac{\partial C}{\partial t} = \left[\left(e^+ - e^-\right) - \nu\kappa\right] N \tag{2}$$

where C now denotes the position vector of the segmenting curve, superscripts $+, -$ denote the values on the two sides of C, N is the normal to C pointing towards the side of C marked $+$ and κ denotes the curvature. To see anisotropicity, look at the limiting case as $\mu \to \infty$. Then C minimizes the limiting functional

$$E_\infty(C) = \int_C \left[\frac{\mu\nu}{2} - \left(\frac{\partial I}{\partial n}\right)^2\right] ds \tag{3}$$

The metric is an anisotropic (non-Riemannian) Finsler metric. It is singular and non-definite, exhibiting space-like and time-like behaviors [10]. Existence of space-like geodesics is an open question.

At the other extreme, as $\mu \to 0$ the behavior is governed by the isotropic Euclidean metric. The curve minimizes

$$E_0(C) = \sum_i \int_{D_i} \left(I - \bar{I}_i\right)^2 + \frac{\nu}{\mu^2}|C| \tag{4}$$

where D_i's are the segments of D and $\bar{I}_i$ is the average value of I in D_i. The curve evolution is given by the equation

$$\frac{\partial C}{\partial t} = \left[\left(\bar{I}^+ - \bar{I}^-\right)\left(\bar{I}^+ + \bar{I}^- - 2I\right) - \frac{\nu}{\mu^2}\kappa\right] \tag{5}$$

The equation is similar to the one used in [8] where the first term is replaced by a constant. The advantage of using the segmentation functional is that it avoids the problem of choosing this constant.

.

Another segmentation functional that leads to isotropic curve evolution is formulated using L^1–norms [11]:

$$E(u,C) = \int\int_{D\setminus C} \|\nabla u\| dx_1 dx_2 + \frac{\nu}{\mu}\int\int_D |u-I| dx_1 dx_2 + \int_C \frac{J_u}{1+\mu J_u} ds \quad (6)$$

where J_u is the jump in u across C, that is, $J_u = |u^+ - u^-|$. In order to implement the functional by gradient descent, curve C is replaced by a continuous function v, the edge-strength function to obtain an approximation

$$E_\rho(u,v) = \int\int_D \{\mu(1-v)^2\|\nabla u\| + \nu|u-I| + \frac{\rho}{2}\|\nabla v\|^2 + \frac{v^2}{2\rho}\} dx_1 dx_2 \quad (7)$$

The gradient descent equations for u and v are:

$$\begin{aligned} \frac{\partial u}{\partial t} &= \left[(1-v)^2\, curv(u) - 2(1-v)\nabla v \cdot \frac{\nabla u}{\|\nabla u\|} - \frac{\nu}{\mu}\frac{(u-I)}{|u-I|}\right]\|\nabla u\| \\ \frac{\partial v}{\partial t} &= \nabla^2 v - \frac{v}{\rho^2} + \frac{2\mu}{\rho}(1-v)\|\nabla u\| \end{aligned} \quad (8)$$

where $curv(u)$ is the curvature of the level curves of u:

$$curv(u) = \frac{u_{x_2}^2 u_{x_1x_1} - 2u_{x_1}u_{x_2}u_{x_1x_2} + u_{x_1}^2 u_{x_2x_2}}{\|\nabla u\|^3} \quad (9)$$

The terms in the bracket in the descent equation for u prescribe the three components of the velocity with which the level curves of u move. The first term is the usual Euclidean curvature term except for the factor of $(1-v)^2$, the second term is the advection induced by the edge-strength function v and the last term prescribes the constant component of the velocity. The sign is automatically chosen such that this component of velocity pushes the level curve towards the corresponding level curve of I. The implied metric is isotropic.

3 Anisotropic Geodesic Flows

It is helpful to start with a slightly more general framework to derive the equation of anisotropic geodesic flow. Let M denote the image domain D when it is endowed with a Riemannian metric, $g = \{g_{ij}\}$. Let C be a curve dividing M into two disjoint submanifolds, M_1 and M_2. Following Cheeger [12], define

$$h(C) = \frac{L(C)}{\min\limits_i A(M_i)} \tag{10}$$

where $L(C)$ is the length of C and $A(M_i)$ is the area of M_i, both being measured with respect to the metric on M. Then the problem of shape recovery may be viewed as the problem of finding the minimum cut of M by minimizing $h(C)$. (Note the dependence of the minimum cut on the size and shape of the image domain due to the term in the denominator.) The gradient flow obtained by calculating the first variation of $h(C)$ is given by the equation

$$\frac{\partial C}{\partial t} = [-\kappa_g \pm h(C)]N_g \tag{11}$$

where κ_g is now the *geodesic* curvature and N_g is the normal defined by the metric; plus sign is to be used if the area bounded by the curve is smaller than its complement, minus otherwise. In the isotropic case with the metric equal to a scalar function θ times the identity metric, the relation between the geodesic curvature κ_g and the Euclidean curvature κ is given by the equation

$$\kappa_g = \frac{1}{\theta}\left[\kappa + \frac{\nabla\theta \cdot N}{\theta}\right] \tag{12}$$

Thus the geodesic curvature includes the advection term. The term $h(C)$ is the component of the velocity which is constant along the curve and varies

.

in magnitude as the curve moves. To implement the flow, the initial curve is embedded as a level curve of a function u and the evolution equation for u is derived such that its level curves move with velocity proportional to their geodesic curvature augmented by a component β, constant along each level curve. If only the motion of the original curve C is of interest, we may assume that all the level curves have the same constant component β equal to $h(C)$, updated continuously as C evolves. However, if the motion of all the level curves is of interest, then the value of h for each level curve must be calculated, making the implementation considerably more difficult. In this paper, only purely anisotropic geodesic flow is studied by setting $\beta = 0$.

The functional for u may be derived using the coarea formula, taking care to define all the quantities involved in terms of the metric g. Let $g^{-1} = \{g^{ij}\}$ be the metric dual to g given by the inverse of the matrix $\{g_{ij}\}$. Let

$$< X, Y >_A = \sum_{i,j} X_i A_{ij} Y_j \tag{13}$$

be the binary form defined by a given matrix A and let

$$\|X\|_A = \sqrt{< X, X >_A} \tag{14}$$

Then the functional for u may be obtained by the coarea formula and has the form

$$\int_M \left[\|\nabla u\|_{g^{-1}} + \beta u \right] = \int_D \left[\|\nabla u\|_{g^{-1}} + \beta u \right] \sqrt{det(g)} \tag{15}$$

where β is assumed to be constant. Here, ∇u is the Euclidean gradient vector $\{u_{x_i}\}$. (In fact, $g^{-1}\nabla u$ is the gradient vector $\nabla_g u$ defined by the metric g and

$||\nabla_g u||_g = ||\nabla u||_{g^{-1}}$.) The evolution equation for u has the form

$$\frac{\partial u}{\partial t} = div_g\left(\frac{g^{-1}\nabla u}{\|\nabla u\|_{g^{-1}}}\right) - \beta \tag{16}$$

where

$$div_g(X) = \sum_i \frac{1}{\sqrt{det(g)}}\partial_i\Big(X_i\sqrt{det(g)}\Big) \tag{17}$$

is the divergence operator defined with respect to g. Eqs. (16) and (17) are valid in arbitrary dimension. The first term in Eq. (16) is the mean geodesic curvature of the level hypersurfaces of u.

In dimension 2, the evolution Eq. (16) for u assumes a fairly simple form and is not much more difficult to implement than in the isotropic case. In dimension 2, after multiplying the right hand side of Eq. (16) by a positive function, we get

$$\frac{\partial u}{\partial t} = curv(u)\|\nabla u\| + \frac{\gamma\|\nabla u\|_K^2 - \frac{1}{2}\|\nabla u\|_Q^2 - \beta\|\nabla u\|_K^3\sqrt{det(K)}}{\|\nabla u\|^2 det(K)} \tag{18}$$

where as before, $curv(u)$ is the Euclidean curvature of the level curves of u, ∇u is the Euclidean gradient of u, $||\nabla u||$ is its Euclidean norm, and

$$\begin{aligned} K &= det(g)g^{-1} \\ \gamma &= \sum_{i,j}\partial_i K_{ij}\partial_j u \\ Q_{ij} &= <\nabla u, \nabla K_{ij}>_K \end{aligned} \tag{19}$$

Comparison with the corresponding equation for the isotropic flow shows that anisotropy does not affect the second order curvature term, but the advection term is more finely tuned. To have the effect of anisotropy on the second order term in dimension 2, more general Finsler metrics must be considered [13].

.

4 Approximation: Riemannian Drums

As in the isotropic case, Eq. (18) is hyperbolic in the direction normal to the level curves so that its solution is capable of developing shocks. A shock-capturing numerical method [14] must be used to implement the equation. An alternative is to convert the minimum-cut problem into an eigenvalue problem as suggested by the Cheeger inequality

$$\lambda \geq \frac{1}{4}\left(\min_{C} h(C)\right)^2 \tag{20}$$

where λ is the second smallest eigenvalue of the Laplace–Beltrami operator. Therefore, instead of minimizing $h(C)$, consider minimizing the Rayleigh quotient

$$\frac{\int\limits_{D} \|\nabla u\|^2_{g^{-1}} \sqrt{det(g)}}{\int\limits_{D} u^2 \sqrt{det(g)}} \tag{21}$$

which is equivalent to solving the eigenvalue problem

$$\Delta_g u + \lambda u = 0, \text{ with Neumann boundary conditions} \tag{22}$$

where

$$\Delta_g u = \frac{1}{\sqrt{det(g)}} \sum_{i,j} \partial_i \left(g^{ij} \sqrt{det(g)} \partial_j u \right) \tag{23}$$

is the Laplace–Beltrami operator. When g is the Euclidean metric, the operator reduces to the ordinary Laplacian and the eigenvalue problem describes the modes of vibration of an elastic membrane. When discretized, the eigenvalue problem takes the form

$$Hu = \lambda M u \tag{24}$$

where u is now a vector, H is the "stiffness" matrix and M is the mass matrix. An important point to note is that Eq. (22) does not involve β, its approximate value is determined automatically by the Cheeger inequality. Another important point to note is that for the approximation to work, an anisotropic metric is essential. In dimension 2, if the metric is isotropic, the numerator in the Rayleigh quotient is independent of g and since we expect g to deviate substantially from the Euclidean metric only near the shape boundary, the denominator is insensitive to g as well. As a result, the eigenvalue problem reduces essentially to the Euclidean case.

The eigenvalue problem (22) is an analytic version of the formulation proposed by Shi and Malik in the framework of graph theory, motivated by the principles of gestalt psychology. They regard the image as a weighted graph by viewing the pixels as vertices and assigning weights to the edges in proportion to the proximity of the corresponding vertices and similarity between the feature values at these vertices. The minimum cut of the graph is defined in some normalized way. There is a standard way to define the Laplacian of a graph from its adjacency matrix [15,16] and approximate the minimum cut problem as the problem of determining the eigenvector corresponding to the second smallest eigenvalue of this Laplacian. Since this eigenvalue is zero if the graph is disconnected, it is called the algebraic connectivity of the graph. For a more detailed comparison between the graph-theoretic formulation and the formulation presented here, see [17]. Note that here too, anisotropicity is essential. Isotropicity would mean that all the edges have the same weight and hence the graph cannot carry any information about the image.

The eigenvalue problem may be approximately solved by one of the spe-

.

cial methods for large sparse matrices such as the Lanczos method [18]. Care must be taken to ensure that the matrix H is symmetric so that the Lanczos method is applicable. One of the ways to ensure this is to derive Eq. (24) by discretizing the Rayleigh quotient (21) instead of Eq. (22). Details of the Lanczos method may be found in [17]. The method is an efficient procedure to find the vector which minimizes the Rayleigh quotient over the vector space $\mathcal{K}_m = \{u_0, M^{-1}Hu_0, (M^{-1}H)^2u_0, \cdots, (M^{-1}H)^m u_0\}$. Here, u_0 is a user-supplied initial vector and m is chosen so that satisfactory numerical convergence is obtained. In principle, the only requirement for the method to work is that the initial vector must have a component along the true eigenvector. However, the greater the number of higher eigenvectors significantly present in u_0, the larger the value of m needed for the method to converge to the second eigenvector. Moreover, as m increases, it becomes harder and harder to orthogonalize the vector space $\mathcal{K}_m$ as required by the Lanczos method. Therefore, the choice of the initial vector is a non-trivial problem.

5. Anisotropic Metrics

In dimension 2, the obvious starting point for intensity images is the matrix

$$\nabla I^\sigma \otimes \nabla I^\sigma = \begin{bmatrix} \partial_1 I^\sigma \partial_1 I^\sigma & \partial_1 I^\sigma \partial_2 I^\sigma \\ \partial_1 I^\sigma \partial_2 I^\sigma & \partial_2 I^\sigma \partial_2 I^\sigma \end{bmatrix} \tag{25}$$

where I^σ denotes the smoothing of the image by a Gaussian filter. There are two problems with the metric defined in this way. First of all, the metric is degenerate since the determinant is zero. This may be remedied by adding a small multiple of the identity matrix to the above matrix. (Shi and Malik solve this problem by

exponentiating the metric.) The second objection is that the length of each level curve of I^σ is just a constant multiple of its Euclidean length. Since we expect the object boundaries to coincide more or less with the level curves, evolving curves will shrink and vanish. A solution to this problem is to divide the augmented matrix by its determinant. The final result is the metric given by the matrix

$$\begin{bmatrix} \frac{1+\alpha\partial_1 I^\sigma \partial_1 I^\sigma}{1+\alpha\|\nabla I^\sigma\|^2} & \frac{\alpha\partial_1 I^\sigma \partial_2 I^\sigma}{1+\alpha\|\nabla I^\sigma\|^2} \\ \frac{\alpha\partial_1 I^\sigma \partial_2 I^\sigma}{1+\alpha\|\nabla I^\sigma\|^2} & \frac{1+\alpha\partial_2 I^\sigma \partial_2 I^\sigma}{1+\alpha\|\nabla I^\sigma\|^2} \end{bmatrix} \tag{26}$$

where α is a constant. Finally, just as in the isotropic case [6], the metric may be raised to some power p. The effect of p is to sharpen the maxima and the minima of the smaller eigenvalue of the metric over the image domain, resulting in sharper edges and corners. In the gradient direction, the infinitestimal length is the Euclidean arclength ds, independent of the gradient. Along the level curves of I^σ, the infinitestimal length is $ds/(1+\alpha||\nabla I^\sigma||^2)^{p/2}$. Thus the metric provides a generalization compatible with the isotropic case as it is usually formulated [6]. Its generalization to vector valued images, for instance to the case where we have a set of transforms $\{I^{(k)}\}$ of the image by a bank of filters, is straightforward. In matrix (26), simply replace $\partial_i I^\sigma \partial_j I^\sigma$ by $\Sigma_k \alpha^{(k)} \partial_i I^{(k)} \partial_j I^{(k)}$. Generalizaton to arbitrary dimension n is obtained by letting the indices i, j run from 1 to n and normalizing the metric by dividing it by the $(n-1)^{th}$ root of its determinant. Of course, determining the weights $\{\alpha^{(k)}\}$ is a difficult problem.

6. Experiments

In the first experiment, different methods considered here are compared from the point of view of smoothing intensity images. In the second experiment, in

.

addition to smoothing an MR image, anisotropic flow is applied to smoothing of the zero-crossings of the Laplacian of the image presmoothed by a Gaussian.

In these experiments, the constant β was set equal to zero and α was chosen so that the smallest value achieved by the smaller eigenvalue of the matrices $\{g_{ij}\}$ over the image domain was equal to a small constant c, less than 1. The closer the value of c is to 1, the closer the metric is to the Euclidean metric. (The Euclidean geodesic flow is a purely curvature-driven flow without advection. The image is eventually smoothed out to uniform intensity.) In the case of the eigenvalue problem, the closer the value of c is to 1, the more the behavior is like a Euclidean drum and the second eigenvector is dominated by the fundamental mode of Euclidean vibration.

In order to clearly bring out the differences among the different methods, a synthetic image with greatly exaggerated noise was used in the first experiment. The image is shown in Figure 1 (top-left) and was created by adding noise to a white ellipse on a black background. The top-right frame shows a horizontal and a vertical cross-section through the middle of the image. The metric was calculated from the filtered image I^σ obtained by filtering the original image by a Gaussian with standard deviation equal to $\sqrt{2}$. I^σ was also used as the initial vector for the geodesic flow as well as for the Lanczos iteration. (Uniformly sampled random noise was also tried as initial u for solving the eigenvalue problem, but the convergence was unacceptably slow.)

Under the isotropic flow, with $\theta = 1/(1 + \alpha||\nabla I^\sigma||^2)^2$ in Eq. (12), all the significant level curves shrank and vanished in a few thousand iterations. The

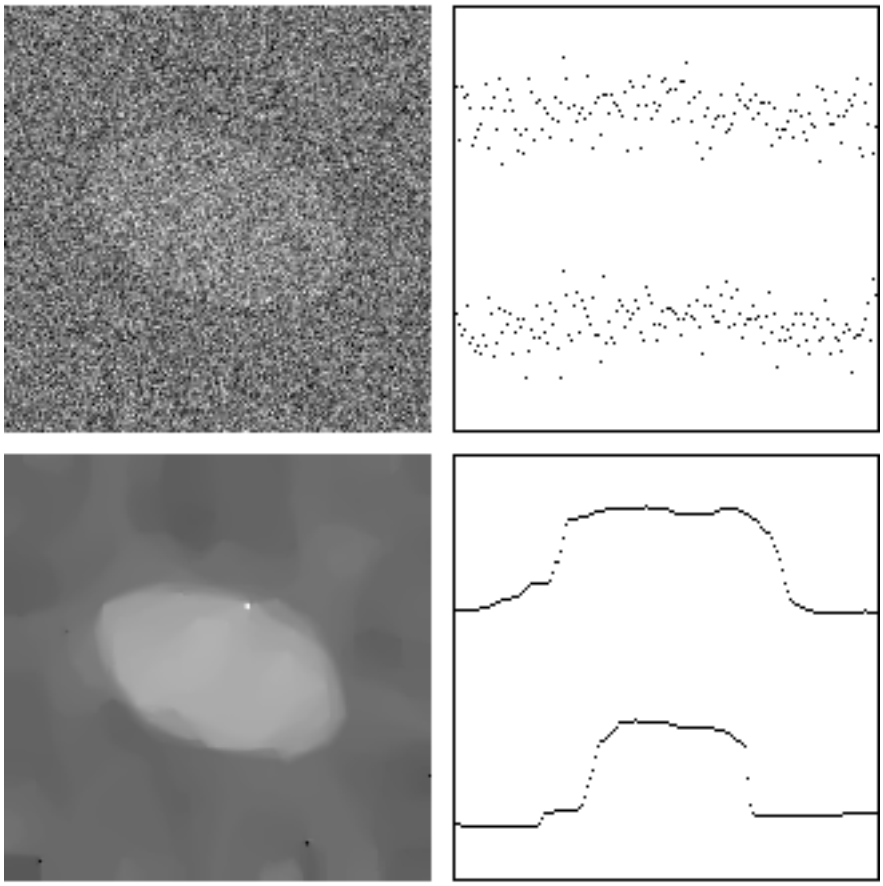

Fig. 1.

bottom frames of Figure 1 show the results of anisotropic geodesic flow. The numerically steady state shown in the figure remained stable even after a few hundred thousand iterations. Sharpening of the edges can be clearly seen in the graph of the cross-sections.

The solution to the eigenvalue problem is shown in the top-row of Figure 2. The figure shows that the method is not as effective as the method of geodesic flow for denoising or deblurring. In fact, the solution is very close to the initial vector I^{σ}.

.

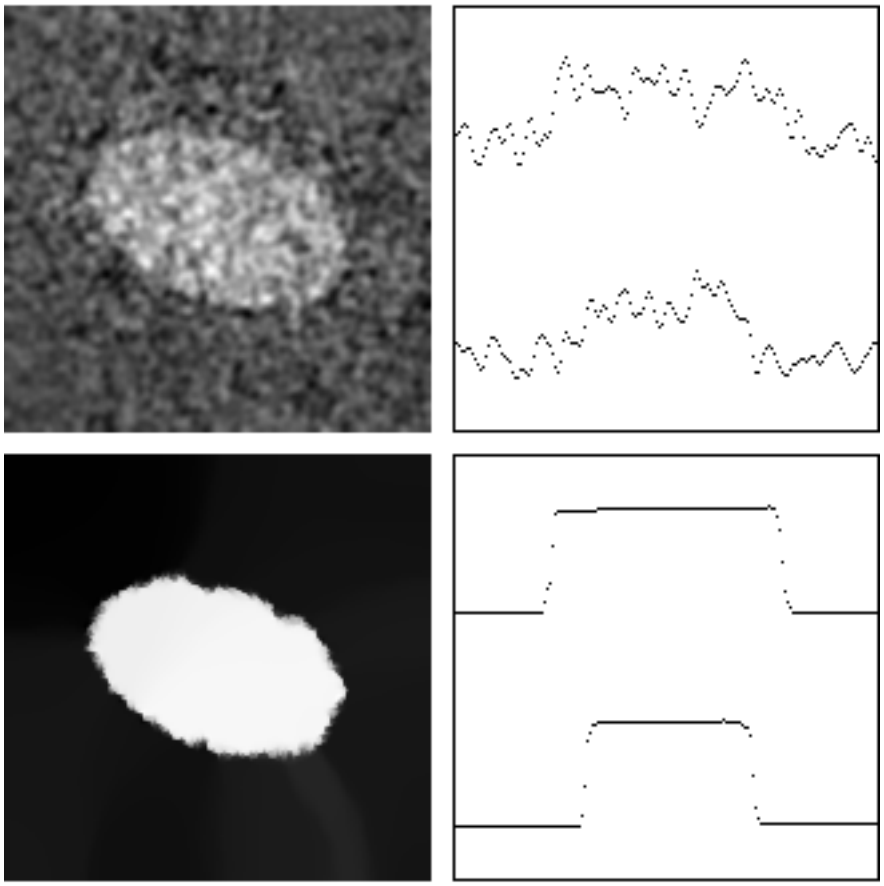

Fig. 2.

The best results were obtained using Eqs. (8) corresponding to the segmentation functional (6) as shown in the bottom row of Figure 2. The advantage of the segmentation functional over the curve evolution formulation is that denoising and edge detection are done simultaneously. The formulation makes it possible for the smoothed intensity u and the edge-strength function v to interact and reinforce each other. In the example shown, u is in fact almost piecewise constant.

Figures 3 and 4 portray the results for an MR image. This is a more difficult image to deal with since the intensity gradient and the curvature vary widely

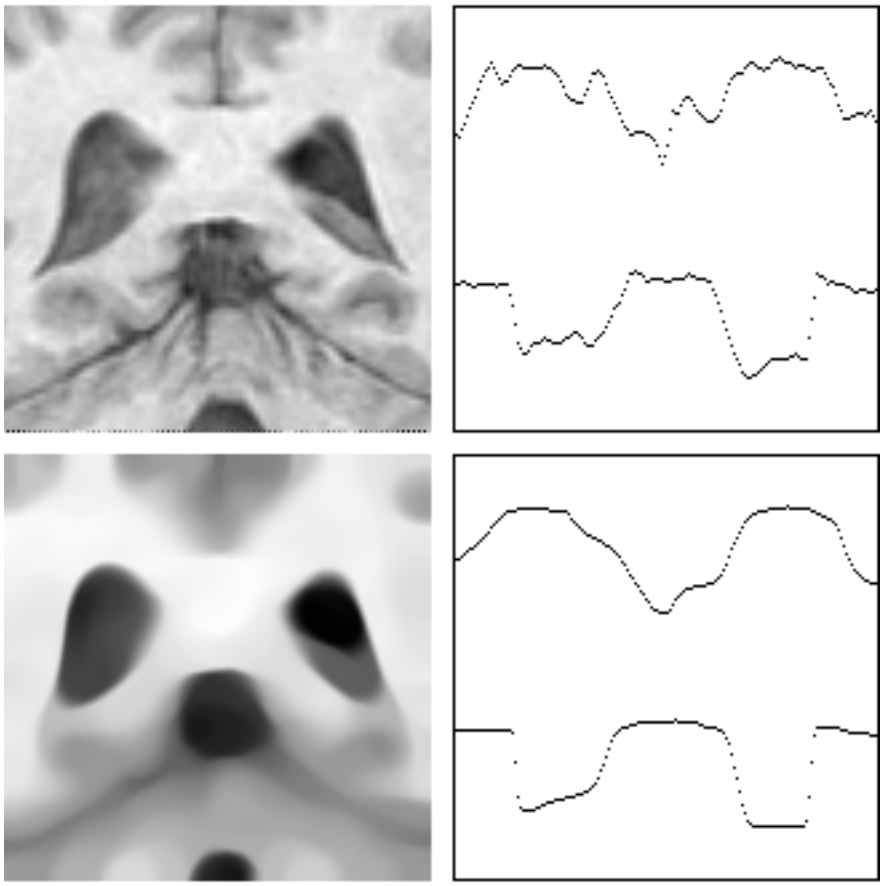

Fig. 3.

along the object boundaries, resulting in varying degrees of smoothing. This is especially true of the thin protrusions and indentations. The top row in Figure 3 shows the original image togetherwith graphs of two horizontal cross-sections. The top graph is a section near the top of the image while the bottom graph is through the two ventricles in the middle. The bottom row shows the effect of smoothing under anisotropic flow using the original image as the initial u as well as for calculating the metric. Figure 4 shows the results of smoothing the zero-crossings of $\nabla^2 I^\sigma$. The case $\sigma = 1/2$ is shown in the top row, the left frame being the initial zero-crossings. The case $\sigma = 3/\sqrt{2}$ is shown in the bottom

.

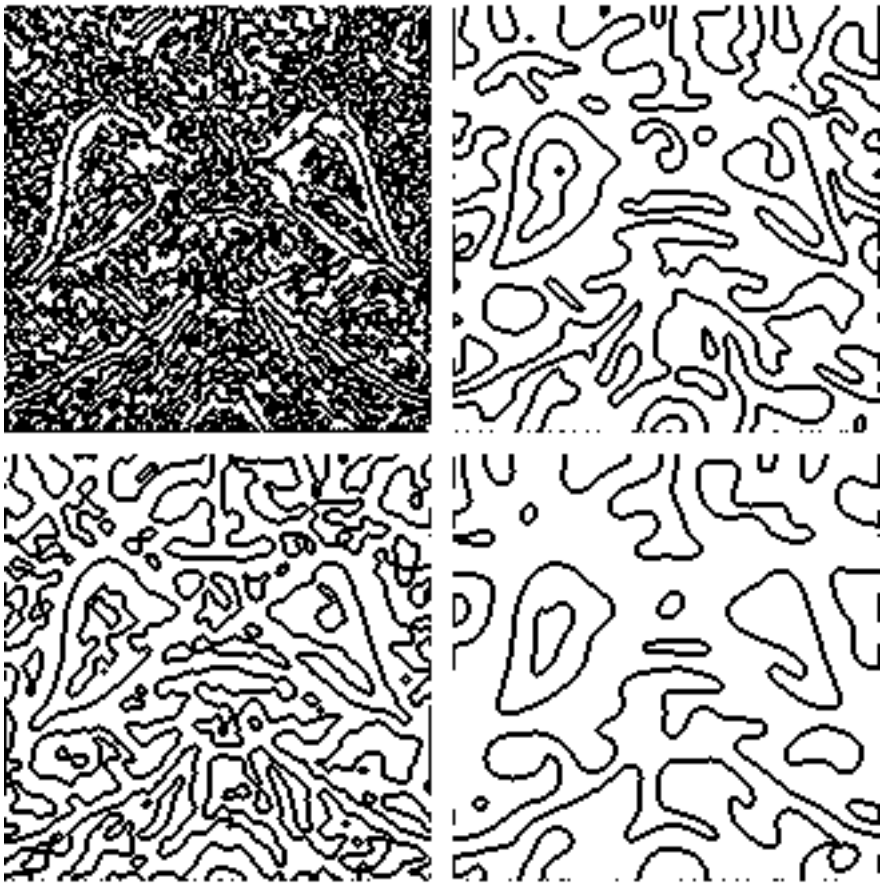

Fig. 4.

row. The anisotropic metric was computed from the original (unsmoothed) image. Stability of the significant boundaries is indicated by the close similarity between the curves in the two figures.

References

(1) M. Kass, A. Witkin and D. Terzopoulos, Snakes: Active Contour Models, International J. of Computer Vision, v.1, 1988.

(2) V. Caselles, F. Catte, T. Coll and F. Dibos, A Geometric Model for Active Contours, Numerische Mathematik 66, 1993.

(3) V. Caselles, R. Kimmel and G. Sapiro, Geodesic Active Contours, Fifth International Conference on Computer Vision, 1995.

(4) S. Kichenassamy, A. Kumar, P. Olver, A. Tannenbaum and A. Yezzi, Gradient Flows and Geometric Active Contour Models, Fifth International Conference on Computer Vision, 1995.

(5) R. Malladi, J.A. Sethian and B.C. Vemuri, Shape Modeling with Front Propagation: A Level Set Approach, IEEE-PAMI 17, 1995.

(6) J. Shah, Shape Recovery from Noisy Images by Curve Evolution, IASTED International Conference on Signal and Image Processing, 1995.

(7) J. Sethian, Numerical Algorithms for Propagating Interfaces, J. of Diff. Geom. v.31, 1990.

(8) H. Tek and B.B. Kimia, Image Segmentation by Reaction-Diffusion Bubbles, Fifth International Conference on Computer Vision, 1995.

(9) J. Shi and J. Malik, Normalized Cuts and Image Segmentation, IEEE Conf. on Computer Vision and Pattern Recognition, 1997.

(10) D. Mumford and J. Shah, Optimal Approximations by Piecewise Smooth Functions and Associated Variational Problems, Comm. on Pure and Appl. Math, v.XLII, n.5, pp.577–684, July, 1989.

(11) J. Shah, A Common Framework for Curve Evolution, Segmentation and Anisotropic Diffusion, IEEE Conference on Computer Vision and Pattern Re:cogntion, June, 1996.

(12) J. Cheeger, A Lower Bound for the Smallest Eigenvalue of the Laplacian, in *Problems in Analysis*, Ed: R.C. Gunning, Princeton University Press, 1970.

.

(13) G. Bellettini and M. Paolini, Anisotropic Motion by Mean Curvature in the Context of Finsler Geometry, Tech. Report, Universita Degli Studi di Milano, 1994.

(14) S. Osher and J. Sethian, Fronts Propagating with Curvature Dependent Speed: Algorithms based on the Hamilton-Jacobi Formulation, J. Comp. Physics, 79, 1988.

(15) R. Merris, Laplacian Matrices of Graphs: A Survey, Linear Algebra and its Applications 197,198, 1994.

(16) B. Mohar, Laplace Eigenvalues of Graphs — A Survey, Discrete Math. 109, 1992.

(17) J. Shah, Segmentation as a Riemannian Drum problem, IEEE International Conference on Image Processing, October, 1998.

(18) Golub and Van Loan, *Matrix Computation*, John Hopkins University Press, 1989.

Figure legends:

Figure 1: Top Right: A synthetic image . Top Left: Horizontal and vertical sections through the middle. Bottom Right: Smoothing by anisotropic geodesic flow. Bottom Left: The two sections.

Figure 2: Top Right: Result of solving the eigenvalue problem. Top Left: The two sections. Bottom Right: Result by L1 functional. Bottom Left: The two sections.

Figure 3: Top Right: An MR image. Top Left: Two horizontal sections. Bottom Right: Smoothing by anisotropic geodesic flow. Bottom Left: The two sections.

Figure 4: Top Right: Zero–crossings of $\nabla^2 I^\sigma, \sigma = 1/2$. Top Left: Smoothing of the zero-crossings by anisotropic flow. Bottom Right: Zero–crossings of $\nabla^2 I^\sigma, \sigma = 3/\sqrt{2}$. Bottom Left: Smoothing of the zero-crossings by anisotropic flow.

.

Biography

The author is a professor of mathematics at the Northeastern University.